SHOCK RECOVERY OF GRANITE WITH A DECAYING SHOCK WAVE: FRAGMENTATION, FORMATION OF STISHOVITE, AND ONSET OF MELTING AT LOW (<20 GPa) SHOCK PRESSURE.

C. Hamann[1], K. Kurosawa[2], F. E. D. Kaufmann[1], H. Ono[2], T. Tada[3], T. Niihara[4], T. Okamoto[2], T. Matsui[2,3], [1]Museum für Naturkunde, Invalidenstr. 43, 10115 Berlin, Germany (christopher.hamann@mfn.berlin), [2]Planetary Exploration Research Center, Chiba Institute of Technology, 2-17-1, Tsudanuma, Narashino, Chiba 275-0016, Japan, [3]Institite for Geo-Cosmology, Chiba Institute of Technology, 2-17-1, Tsudanuma, Narashino, Chiba 275-0016, Japan. [4]Department of Applied Science, Okayama University of Science, 1-1 Ridaicho, Kita-ku, Okayama, Okayama 113-8656, Japan.

Introduction: Impact cratering has governed the evolution of planetary crusts since their initial formation in the early solar system. To understand their evolution, knowledge of the response of planetary materials to impact is thus mandatory. It is also needed to interpret shock metamorphism of samples from terrestrial impact structures or of samples from other planetary bodies, e.g., meteorites or material retrieved in space missions.

Laboratory shock-wave experiments have been essential in characterizing the response of planetary materials to shock compression. They provide insight into the shock metamorphism of solids and are the basis of classification schemes of progressive shock metamorphism—i.e., the definition of distinctive 'shock stages' as advocated, e.g., by [1]. However, recovery of shocked material that documents in one single sample large shock-pressure ranges that cover several shock stages as well as the transitions between them has been challenging in conventional, flyer plate-based shock-recovery experiments and two-stage light-gas gun impact experiments [2]. In addition, excavation of material due to crater formation in impact experiments makes it difficult to assess the effects of friction and plastic deformation on impact melting. This process is thought to cause melting of material along shear zones at shock pressures far below those typically required for the onset of melting [3, 4], yet a detailed experimental investigation of the onset and nature of shear-induced melting is currently lacking.

Here, we report on shock-recovery experiments that make use of decaying hemispherical (instead of planar) shock waves to investigate shock metamorphism, shear-induced melting, and fragmentation of granite shocked to continuously decreasing pressures between 18 and 1 GPa, which is characteristic for the majority of material in natural impacts [1]. As our setup produces singular shock compression and a large degree of shear (i.e., it avoids further "ring-up" compression of the sample by compressive waves reflected from the sample container), we can investigate the significance of heating due to plastic deformation around the epicenter.

Materials and Methods: 30-mm-wide, 24-mm-long cylinders of Inada granite from Ibaraki, Japan were inserted into titanium containers and covered by 3-mm-thick titanium front plates (Fig. 1A). The front plates of

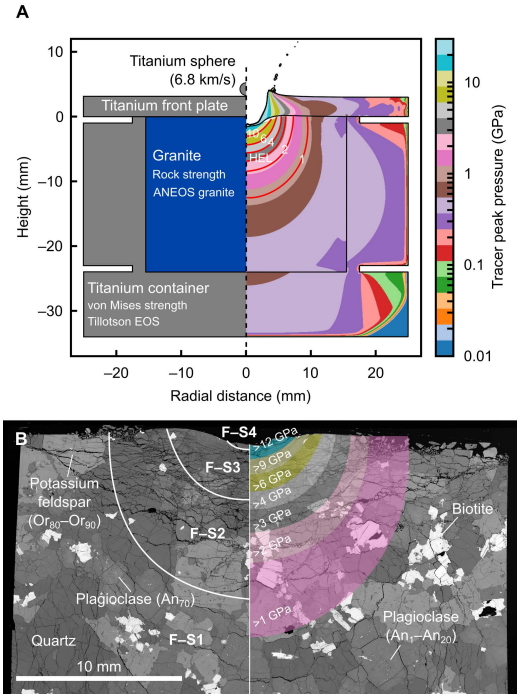

Fig. 1 A Experimental design and peak pressure distribution for a time step at which the shock wave has engulfed the entire granite target. **B** BSE image mosaic of the upper half of the recovered sample. Shock stages F–S1 to F–S4 [1] and isobars calculated from the iSALE model are shown for reference.

the containers were impacted by titanium or polycarbonate projectiles using a two-stage light-gas gun operated at the Planetary Exploration Research Center, Chiba Institute of Technology, Japan. Here, we report on shot #494 (2-mm-diameter titanium projectile; 6.8 km/s impact velocity), for which spatial and temporal distributions of shock pressures and temperatures were estimated from a iSALE-2D model that employed the ANEOS [5] for granite [6], the Tillotson EOS for titanium [7], and similar calculation settings as used in previous studies [8]. Thin sections cut perpendicular to the epicenter were investigated by optical microscopy, SEM, EMPA, and Raman spectroscopy at Museum für Naturkunde Berlin, Germany. The free image analysis software ImageJ was used to obtain cumulative fragment size–frequency distributions (cf. [9]) as a function of depth below the point of impact from BSE image mosaics taken at 250–750× magnification.

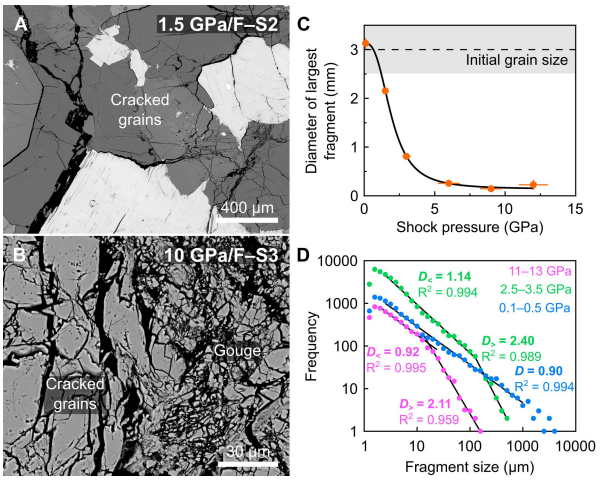

Fig. 2 A, B Representative BSE images of fragmentation in F–S2 (~1.5 GPa) and F–S3 (~10 GPa) material. **C** Diameter of largest fragment vs. pressure. **D** Evolution of fragment size–frequency distributions for different shock zones.

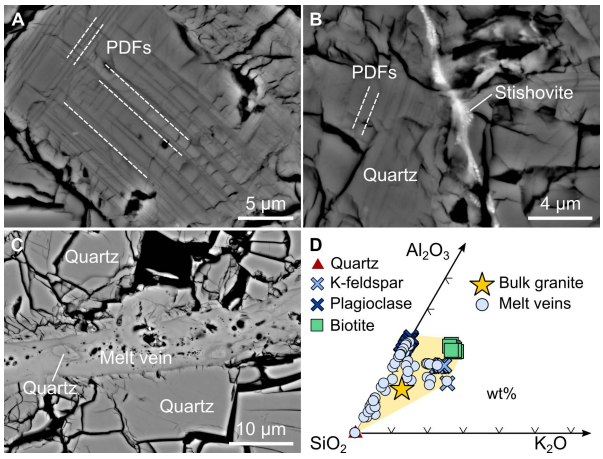

Fig. 3 A–C Representative BSE images of PDFs in quartz (A), stishovite (B), and melt veins (C) in shock stage F–S3/4 material. **D** Chemical compositions of the melt veins.

Results and Discussion: The iSALE model suggests that the shock pressure in the sample reached a maximum of about 18 GPa and 700 K (i.e., shock stage F–S3/4) at the point of impact (Fig. 1A). Successive attenuation of the shock wave resulted in hemispherical zones in which the shock pressures decreased within ~6 mm to about 3 GPa (F–S2), i.e., close to Hugoniot elastic limit, and within ~11 mm to 1 GPa (F–S1).

A lens-shaped zone of intense fragmentation (Fig. 1B) can be recognized in the thin sections up to a depth of 5–6 mm (~3 GPa). Fractures within and on the sides of this lens are of similar appearance as those described by [10]. The intensity of fragmentation increases with increasing shock pressure (Fig. 2A–C): Material shocked to ≤1 GPa exhibits fractures of hundreds of micrometers length that typically follow grain boundaries. Fractures become more numerous and shorter in material compressed to 1–3 GPa; the number of intragranular fractures increases here and tensile fractures start to appear. Material at >3 GPa shows abundant intragranular fractures and significantly smaller fragment sizes (Fig. 2B, C); gouge-like deformation bands with grain sizes <5 µm start to appear (Fig. 2B). Cumulative fragment size–frequency distributions obtained from 3–18 GPa material (Fig. 2D) yield *D* values (slope of frequency vs. fragment-size curve) of 2.11–2.40, which is in the range of tectonically deformed granite [9]. A second population of fragments with smaller sizes (e.g., ≤10 µm close to the epicenter; Fig. 2B) and *D* values of 0.92–1.14 also exists here that probably formed by attrition concentrated in the deformation bands [9]. *D* value analysis and comparison to impact-fragmentation models are ongoing.

The distribution of shock effects at various depths in the recovered sample is mostly consistent with the classification scheme of [1]. Around 5 GPa, kink bands in biotite appear, followed by undulatory extinction in quartz and feldspar at 5–8 GPa. Planar fractures in quartz appear at ≥8 GPa, whereas quartz shocked to ≥12 GPa displays two or three sets of well-developed planar deformation features (Fig. 3A) and veins of a dense silica polymorph (Fig. 3B) that we tentatively identify as stishovite (cf. [11]). In a companion abstract, Tada et al. [this meeting] also report on feather features developed in quartz shocked to 8–18 GPa. Furthermore, 10–20 µm thick, several hundreds of micrometers long, vesicular, monomineralic (e.g., quartz) or polymineralic (e.g., quartz–feldspar) silicate melt veins exist along former grain boundaries and within heavily fractured grains in nominally F–S3 or F–S4 material (Fig. 3C, D).

Conclusions: Our experiments demonstrate the significance of shear-induced melting, which forms narrow melt veins in granite shocked to moderate pressures (<20 GP) that are nominally incommensurate with incipient melting (thought to start at >40–50 GPa).

Acknowledgments: We thank the developers of iSALE, including G. Collins, K. Wünnemann, B. Ivanov, J. Melosh, and D. Elbeshausen. We also thank T. Davison for the development of pySALEPlot.

References: [1] Stöffler D. et al. (2018) *Meteorit. Planet. Sci., 53,* 5–49. [2] Nagaki K. et al. (2016) *Meteorit. Planet. Sci., 51,* 1153–1162. [3] Kenkmann T. et al. (2000) *Meteorit. Planet. Sci., 35,* 1275–1290. [4] Kurosawa K. and Genda H. (2018) *GRL, 45,* 620–626. [5] Thomson S. and Lauson H. (1972) SNL Rep., SC-RR-71 0714. [6] Pierazzo E. et al. (1997) *Icarus, 127,* 408–423. [7] Tillotson J. H. (1962) Rep. No. GA-3216, General Atomic, San Diego. [8] Kurosawa K. et al., in revision. [9] Stünitz H. et al. (2012) *J. Struct. Geol., 32,* 59–69. [10] Polanskey C. A. and Ahrens T. J. (1990) *Icarus, 87,* 140–155. [11] Mansfeld et al. (2017) *Meteorit. Planet. Sci., 52,* 1449–1464.